

# RSC Advances



This is an *Accepted Manuscript*, which has been through the Royal Society of Chemistry peer review process and has been accepted for publication.

*Accepted Manuscripts* are published online shortly after acceptance, before technical editing, formatting and proof reading. Using this free service, authors can make their results available to the community, in citable form, before we publish the edited article. This *Accepted Manuscript* will be replaced by the edited, formatted and paginated article as soon as this is available.

You can find more information about *Accepted Manuscripts* in the [Information for Authors](#).

Please note that technical editing may introduce minor changes to the text and/or graphics, which may alter content. The journal's standard [Terms & Conditions](#) and the [Ethical guidelines](#) still apply. In no event shall the Royal Society of Chemistry be held responsible for any errors or omissions in this *Accepted Manuscript* or any consequences arising from the use of any information it contains.

# Novel catalyst PTMA-PILC: structural properties and catalytic performance for the bioethanol dehydration to ethylene<sup>□</sup>

Xianmei Xie<sup>\*a</sup>, Zheng Li<sup>a</sup>, Baoru Li<sup>a</sup>, Xu Wu<sup>a</sup>, Xia An<sup>a</sup>

**Abstract:** Novel Phosphomolybdic acid-Pillared interlayer clay (PTMA-PILC) catalysts were prepared by three steps of acid treatment, ion-exchanging and impregnation method. The resulted catalysts were initially characterized by a combination analysis of XRD, FT-IR, TG, NH<sub>3</sub>-TPD, Pyridine-IR, TEM, and N<sub>2</sub> adsorption-desorption. Characterization results indicated that the sandwich structure of the montmorillonite were delaminated on the acid treatment, resulting in the surface area to 335 m<sup>2</sup>/g and plate-like particles. After the ion-exchanging and impregnation method, the stratified structure was restored surprisingly. The strong and weak acidity contents were also changed. The catalytic properties of the series of catalysts were tested in the dehydration of ethanol to ethylene. A significant improvement on catalytic activity was observed in the dehydration of ethanol (30 vol %) to ethylene on the synthesized PTMA-PILC catalyst, wherein 93.2% conversion and 99.1% selectivity of ethylene were achieved at 300 °C. The improved activities were attributed to the layer structure and balance of Lewis and Bronsted acid sites.

**Keywords:** Acid treatment; PILC (Pillared interlayer clay); Bioethanol dehydration to ethylene

## 1 Introduction

Ethylene is one of important fine chemicals for petrochemical industry and it is mainly produced from thermal cracking of petroleum or nature gas feedstock<sup>1</sup>. With the shortage of natural resource and energy and the soaring prices of crude oil, production of petrochemicals from a non-petroleum, environment friendly feedstock has sparked a lot of interests and the development of efficient ethylene production processes are one of the challenging research areas<sup>2-3</sup>. Compared with the traditional process, the ethylene production from the dehydration of ethanol is economically feasible with higher purity<sup>4</sup>. Moreover, the utilization of ethanol from biomass fermentation instead of petroleum as chemical feedstock may facilitate the reduction of CO<sub>2</sub> emission which was a crucial problem in the chemical industry<sup>5</sup>. In order to make ethanol dehydration more industry-friendly, scientists and researchers have developed different catalysts to enhance ethylene yield and lower reaction temperature and the concentration of alcohol. The catalysts for acid-catalyzed alcohol dehydration can be classified as four categories<sup>4</sup>: phosphoric acids<sup>6</sup>, oxides<sup>7</sup>, zeolites<sup>8-9</sup> and heteropolyacids<sup>10-11</sup>. As for earlier  $\gamma$ -Al<sub>2</sub>O<sub>3</sub> catalyst, ethanol dehydration required higher reaction temperature (400-450 °C) and offered lower ethylene yield (80%)<sup>12-13</sup>. The obvious disadvantage was a purification process of bioethanol with high energy consumption because of the poor catalytic properties when bioethanol solution contained large amount of water as reactant over Al<sub>2</sub>O<sub>3</sub> catalyst was used<sup>1</sup>. HZSM-5 zeolite was concerned

recently and a ethanol conversion of 98% at lower temperature (300 °C) was reported<sup>14-15</sup>. However, deactivation caused by coke deposition easily occurred on HZSM-5 zeolites for ethanol dehydration because of its smaller pore size and strong acidic properties<sup>16</sup>. Arias *et al.*<sup>17</sup> reported the dehydration of ethanol over SAPO-11 catalyst. The yield of ethylene achieved about 90% at 320 °C. In order to improve the yield of ethylene, Zhang *et al.*<sup>13</sup> chose metal doped-SAPO as catalyst, the best yield of ethylene was 92.3% for dehydration of ethanol at 350 °C over Ni-substituted SAPO-34. Unfortunately, the yield only increased about 2% at the cost of improving temperature by 30 °C. So far dehydration reaction of bioethanol to ethylene has been studied extensively. Supported heteropoly acids (HPA) have become popular because of their redox natures, super acidic properties and the keggin structure. They function ubiquitously in homogeneous as well as heterogeneous catalytic reactions<sup>18-23</sup>. However, HPA has several shortcomings such as instability, small specific surface area and aggregating easily. This problem can work out by loading heteropolyacids on the supporters of high surface area and stable structure.

Over the past decades, considerable attention has been paid to montmorillonite (MMT) as catalyst and catalyst supports because of their porosities, reactivities and thermal stabilities. Montmorillonite, a 2:1 clay mineral with two tetrahedral silica layers of Mg or Al to form an octahedral metal oxide structure. The layers are separated from each other by an interlayer or a gallery containing cations (Na<sup>+</sup>, K<sup>+</sup>, Ca<sup>2+</sup>, etc.), which balance the excess negative charges created by natural substitution of some atoms forming the crystal<sup>24</sup>. These cations are exchangeable, which is the reason for the high adsorption capacity of MMT for cations (cation exchange capacity, CEC). MMT in its natural form does not show much catalytic activity. To improve its porosities and stabilities, pillaring method is often employed by intercalating large organic or inorganic molecules<sup>25</sup> between the silicate layers of clays. On the use of Pillared interlayer clays (PILCs) as support of the conventional metal catalysts, most of them using Al-metal pillared

<sup>a</sup>School of Chemistry and Chemical Engineering, Taiyuan University of Technology, Taiyuan 030024, China

clays. PILC also exhibited great importance in the porous solids family<sup>26-27</sup>. In the traditional method,  $\text{Al}_{13}^{7+}$  ( $[\text{AlO}_4\text{Al}_{12}(\text{OH})_{24}(\text{OH}_2)_{12}]^{7+}$ ) units were inserted into the untreated MMT. The polymer  $\text{Al}_{13}^{7+}$  has a Keggin structure. It consists of 12 octahedral Al, arranged in four groups of three octahedra around a central  $(\text{AlO}_4)$  tetrahedron<sup>28</sup>. However,  $\text{Al}_{13}^{7+}$  can not be distributed completely since this hydroxyl polymer can not be replaced by other cations as the chemical bonds can be formed between the  $\text{H}^+$  around the OH of  $[\text{Al}(\text{OH})_6]$  and the  $\text{O}^{2-}$  of the MMT silicate layers.

In this study, Na-Montmorillonite (Na-MMT) precursors were modified by sulfuric acid firstly. The acid treatment can enhance the unique properties of MMT. The skeleton crystal lattice would be dehisced and the interlayer space of the MMT would be increased obviously. MMT would be pillared by polymer  $\text{Al}_{13}^{7+}$  unit. The structure of MMT would be restored because of its “memory effect”. We further improved catalytic properties by supporting Phosphomolybdic (PTMA) on the modified MMT which has large surface area. These modified MMT were served as a robust catalyst in the simulated bioethanol (30 vol%) dehydration to ethylene with enhanced performances.

## 2 Experimental

### 2.1 Chemicals

Sodium montmorillonite (Na-MMT) was supplied by Zhejiang Sanding Technology Co., Ltd., China. The chemical composition of Na-MMT was shown in Table S1. All chemicals used in this study, including NaOH,  $\text{H}_2\text{SO}_4$  (98%),  $\text{AlCl}_3 \cdot 6\text{H}_2\text{O}$  (Shanghai Jinshan Chemical plant) and phosphomolybdic acid (Tianjin Kaida plant), were of analytical reagent grade.

### 2.2 Catalysts preparation

The acid treatment of the MMT: the purified Na-MMT (10 g), was dispersed in 40 mL  $\text{H}_2\text{SO}_4$  with 25 percent in mass and refluxed at 70 °C for 5 h. Then the slurry was cooled, filtered and washed thoroughly with distilled water, the MMT was dried at 80 °C for 6 h and named AT-MMT (Acid treatment-montmorillonite).

Preparation of the Pillared montmorillonite: The pillaring agent was prepared from the hydrolysis of  $\text{AlCl}_3$  solutions with 0.2 mol/L NaOH. Sodium hydroxide was added to the aluminium chloride solution under vigorously stirring at room temperature. The titration was stopped when the  $\text{OH}^-/\text{Al}^{3+}=2.4$ , followed aging at 70 °C for 24 h. The MMT suspension with 10 g of AT-MMT and 400 mL of distilled water was prepared firstly and stirred for 1h. A certain amount of pillaring agents which were got by Ion-Exchange Capacity were added into the clay slurry, then the reaction mixture was stirred continuously for 2 h under vigorous stirring at room temperature. After aging for 24 h at 60 °C, the pillared clay was washed until total elimination of chloride ions, dried at 70 °C for 24 h, named PILC(a) [(Pillared interlayer clay)(a)] and finally calcined at 400 °C for 3 h, named PILC (Pillared interlayer clay).

Preparation of the PTMA-PILC: 10 g of PILC and 0.5 g of PTMA (phosphomolybdic acid) were weighed separately. The

PTMA was dissolved in 10 mL distilled water. The PTMA solution was added slowly into the suspension liquid of PILC with constant stirring. The sample was further dried in an oven at 80 °C in order to remove water completely and the dried catalyst sample was kept in a sealed bottle. Prior to use, the sample was dried in an oven to remove the moisture.

The catalyst characterization and catalytic performance test were listed in Supporting Information.

## 3 Results and discussion

### 3.1 XRD

Fig. 1 shows the XRD patterns of the Na-MMT, AT-MMT, PILC (a), PILC and PTMA-PILC catalysts. The lines at 7.08° and 19.77° of Na-MMT corresponding to the support 001 and 100 reflections and the lines at 2θ of 26.67° belonged to quartz impurities. The obtained XRD pattern for the Na-MMT exhibits a basal distance ( $d_{001}$ ) of 1.26 nm, a typical of Na-MMT. However, the pattern for the 001 and 100 of the AT-MMT disappeared. It was deduced that acid treatment had dramatically changed the structure of the MMT and the lamellar had been delaminated. After  $\text{Al}_{13}^{7+}$  was inserted into the interlayers of MMT, rather to our surprises, the structure and elementary property of MMT restored and the interlayer spacing  $d_{001}$  of PILC (a) increases from 1.26 nm to 1.70 nm, indicating a great expansion of the 001 interlayer distance. However, the height of the  $\text{Al}_{13}^{7+}$  was 0.9 nm<sup>29</sup> and we can get the layer thickness of the AT-MMT was 0.8 nm (Fig. S2), which is slightly lower than the previous researches<sup>30</sup>. It may be due to the reduction of the MMT layer thickness which resulted from dealumination of the aluminium-oxygen octahedron structure. After calcined at 400 °C, massive hydroxyl groups took off. The thermal treatment causes the transformation of the interlayer compounds from polycations to oxides. These results were in agreement with the chemical composition measured by XRF as shown in Table S2, in which the amount of  $\text{Al}_2\text{O}_3$  and Al/Si molar ratio in PILC were higher than AT-MMT. The interlayer spacing  $d_{001}$  of PILC reduced from 1.76 nm to 1.40 nm, may due to the reduction of the MMT layer thickness. The two-step method pillaring process that the firm molecular skeleton of the MMT were stripped by the acid treatment firstly and then recombined with the help of the  $\text{Al}_{13}^{7+}$  benefited the active centre dispersing uniformly in the MMT carrier. There are not strong variation of the patterns and peaks from other crystalline impurities for the PTMA-PILC catalyst, indicating that the PTMA merely loaded onto the surface and in the interlamination of the PILC. The schematic models of the two-step method pillaring process of PTMA-PILC and traditional methods of PILC(b) [(Pillared interlayer clay)(b)] were shown in Scheme 1.

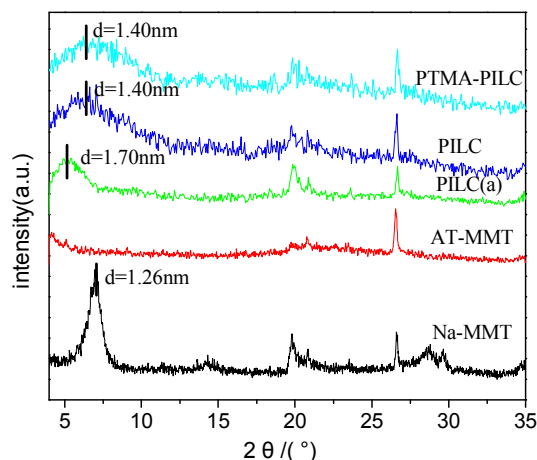


Fig. 1 XRD patterns of different catalysts

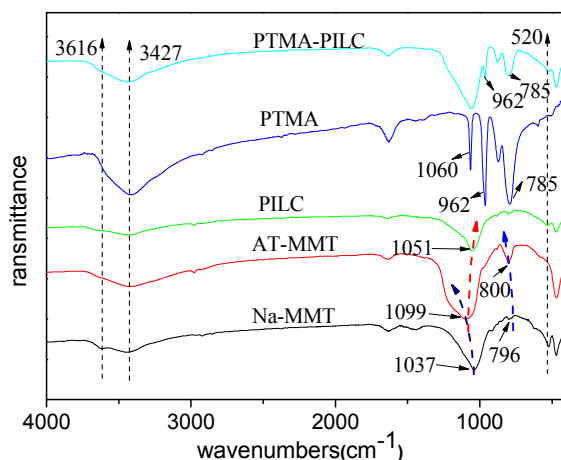
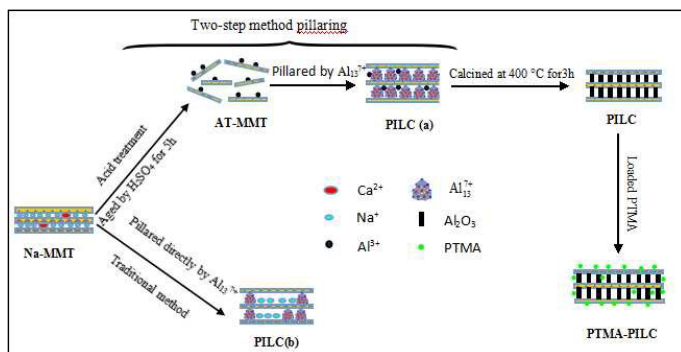


Fig. 2 FT-IR spectra of different catalysts.



Scheme 1. Schematic model of the synthetic process of PTMA-PILC.

### 3.2 FT-IR

In the FT-IR spectra of the Na-MMT samples, the peaks at 1037 and 520  $\text{cm}^{-1}$  were attributed to Si-O in-plane stretching and Si-O bending vibrations respectively. The band at 796  $\text{cm}^{-1}$  attributed to the presence of cristobalite. The broad band at 3427  $\text{cm}^{-1}$  belonged to the stretching vibration of the hydroxyl groups of water molecule. The band at 3616  $\text{cm}^{-1}$  was assigned to OH-Al bonds of octahedral cations<sup>31</sup>. In the FT-IR spectra of the AT-MMT, the position and shape of the band changed slightly. The band at 1037  $\text{cm}^{-1}$  was shifted to higher wavenumber 1099  $\text{cm}^{-1}$  and the peak at 520  $\text{cm}^{-1}$  disappeared. This was in agreement with the results of XRD analysis which showed acid treatment had dramatically changed the structure of the MMT. The band at 796  $\text{cm}^{-1}$  was shifted to 800  $\text{cm}^{-1}$  and its intensity increased significantly after acid treatment. By pillaring, the band at 1099  $\text{cm}^{-1}$  was shifted to lower wavenumber 1051  $\text{cm}^{-1}$ , the band at 3427  $\text{cm}^{-1}$  was broadened, which was interpreted as the effect of pillaring<sup>20</sup>. The increase in the intensity of the band at 3616  $\text{cm}^{-1}$  was related to the presence of aluminum oxocations in the samples. This finding confirmed the lamellar was recombined and the aluminium oxide was intercalated into the interlayers of the MMT. For the pure PTMA, the characteristic absorption bands of Mo-O (785  $\text{cm}^{-1}$ ), P-O (962  $\text{cm}^{-1}$  and 1060  $\text{cm}^{-1}$ ) were clearly observed. For the PTMA-PILC, the main characteristic peaks of the PTMA showed up, proving that the novel supported catalyst had been synthesized.

### 3.3 N<sub>2</sub> adsorption-desorption isotherms

Nitrogen adsorption-desorption isotherms and the pore size distribution (inset) of different catalysts were shown in Fig. 3. The size and shape of the hysteresis loops were changed under acid treatment. In the cases of Na-MMT, a typical H4 hysteresis loop can be suggested because the branches of the adsorption and desorption are nearly horizontal and parallel in a wide range of  $P/P_0$ , which is indicative of the narrow slit-like pores<sup>32</sup>. At low values of  $P/P_0$ , the Nitrogen adsorption-desorption isotherms of the Na-MMT shifted to x-offset, showing little intercrystalline micropore. But AT-MMT exhibited a type I, showing that there is strong interaction with nitrogen. It is because that  $\text{Na}^+$  ions were leached out and replaced by hydrogen ions and the edges of the platelets became more opened, particles were denser due to delaminating of the MMT laminar structure. Generally, The loosely coherent plate-like particles are interpreted for H3 hysteresis loop<sup>33</sup>. At high values of  $P/P_0$ , after activated by sulfuric acid, a gradual change of the isotherm from H4 to H3 hysteresis loop is observed. In consequence, the delamination of the MMT laminar structure and increase of the number of layers per stack were proved existing. This explanation is well confirmed from the BJH pore size distribution (inset). As is shown, the Na-MMT shows very similar pore size distributions and the peak pore size is centered at about 3.7 nm. On the contrary, AT-MMT shows very broad pore size distribution and a clear shift toward larger pore size of 9.1 nm. More mesopores are created over the acid treatment and the pore size distribution becomes wider, which due to the partial destruction of the layered MMT structure. After pillaring reaction and loaded process, the isotherms recovered to the shape of H4 and the pore size shifted to the original size (3.7 nm), showing that the sandwich structure of MMT were restored. These processes quite fit in with the analysis of XRD and FT-IR. The calculated textural data of different catalysts are summarized in Table S2. In the case of the Na-MMT, its surface area is about 21  $\text{m}^2/\text{g}$ . But unbelievably, after activated by sulfuric acid, its BET surface area increased to about 335  $\text{m}^2/\text{g}$ . It is certainly due to the massive micropores and stacking pores. Moreover, the surface area of PILC reduced to 301  $\text{m}^2/\text{g}$ . It was because that the  $\text{Al}_{13}^{7+}$  had accessed

the layers of MMT and transformed non-crystalline oxides after calcined. There is no any significant change beyond that the surface area decreased to 253 m<sup>2</sup>/g for the PTMA-PILC. It merely because the PTMA was loaded on the surface of PILC catalyst.

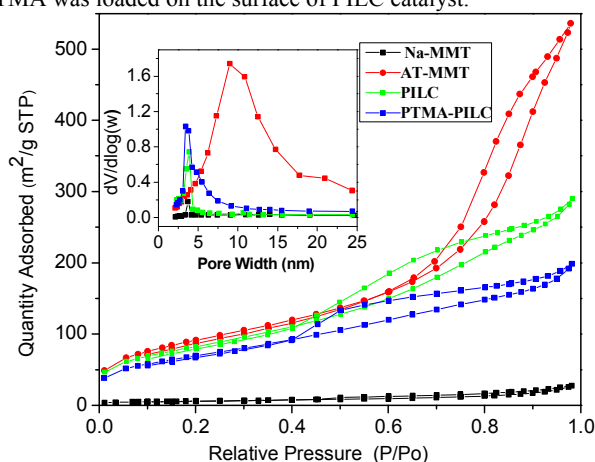
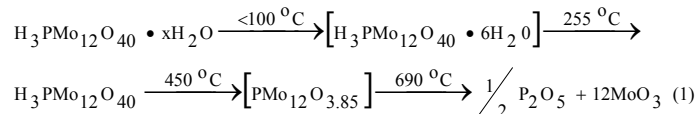


Fig. 3 N<sub>2</sub> adsorption-desorption isotherms and pore size distributions (inset) of different catalysts

### 3.4 TG-DTG analysis

The TG-DTG curve ( Fig. S3) revealed that a weight loss procedure for all the samples in the temperature below 100 °C corresponding to hydration water adsorbed on the surface or in the MMT layers. For Na-MMT, a mass loss of 5.12% was observed at 78 °C. However, the mass loss percentages of AT-MMT, PILC and PTMA-PILC were 3.66%, 3.46%, and 2.80%, respectively. The weight loss of hydration water decreased obviously and the weightlessness peak was shifted from 78 °C to 90 °C for the modified MMT. The presence of large quantities of hydrated cation were attributed to the gallery containing cations (Na<sup>+</sup>, Ca<sup>2+</sup> etc.). The lamellar were delaminated and the bonding forces between the interlayer weakened after acid treatment, so the hydrated cation adsorption reduced. The negative charges were further balanced by the Al<sub>13</sub><sup>7+</sup>, and the Na-MMT was converted from hydrophilic to hydrophobic. The weight loss procedure between 570 °C and 628 °C was ascribed to the dehydroxylation of structural OH groups which located in the tetrahedral sheets of 2:1 MMT layers. Comparing the Na-MMT and modified MMT results, this peak shifted to lower temperature and the mass loss percentages also reduced from 6.49% to 5.83% to 2.5% to 1.88%. The skeleton crystal lattice of Na-MMT were dehisced in the acid treatment process, so the OH groups could easily expose and be removed. After pillared by acid solution of Al<sub>13</sub><sup>7+</sup>, the hydroxyl groups were removed more easily since the chemical bond were formed between the H<sup>+</sup> around the OH of Al<sub>13</sub><sup>7+</sup> and the O<sup>2-</sup> of the MMT silicate layers. On PILC catalyst, there was a weight loss at 449 °C which due to the dehydroxylation of the polyhydroxy aluminium cations<sup>25</sup>. For the PTMA-PILC catalyst, the first weight loss is near 90 °C and was related to the adsorbed water and the second mass loss step occurs at 255 °C was attributed to the bound water on the phosphomolybdic acid. As the temperature rise up to 450 °C, the acidic protons would lose and the Keggin structure of the PTMA begin to decompose. With temperature increasing to 690 °C,

P<sub>2</sub>O<sub>5</sub> and the MoO<sub>3</sub> were formed. Thermal decomposition process of the Phosphomolybdic acid was shown in Eq. (1).



### 3.5 NH<sub>3</sub>-TPD

NH<sub>3</sub>-TPD was used to characterize the acidic properties of the samples. The desorption temperature indicates the acid strength of sample. The higher desorption temperature is, the stronger the acid strength is. The acid amounts corresponding to the amounts of adsorbed NH<sub>3</sub> were estimated from the areas underlying the NH<sub>3</sub>-TPD curves. As shown in Fig. 4, there are two ammonia desorption peaks for all the catalysts. The low temperature desorption peaks centered near 90 °C were attributed to weak acid sites present as surface hydroxyl groups and other acids. As it was shown for the first peak in Fig. 4, the number of weak acid sites of the samples was enhanced from 0.086 to 0.112 mmol/g (Table S3) after acid treatment, but the acid strength did not change. This enhancement was more higher for the PILC as the polycations transformed into non-crystalline aluminium oxide. The weak acid sites was further enhanced to 0.178 mmol/g. For the second peak, however, the dehydroxylation of structural OH groups which located in the MMT framework would take place between 570 °C and 628 °C. It's important to note that the changes of TG and DTG curves for the modified MMT were completely consistent with the change of NH<sub>3</sub> desorption peaks. So the desorption peak appeared at high temperature on account of the desorption of water from condensation of MMT framework.

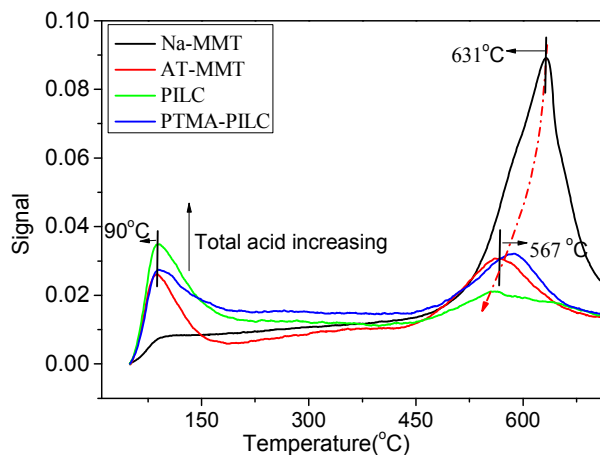


Fig. 4 NH<sub>3</sub>-TPD profiles of different catalysts.

### 3.6 Pyridine-IR

The IR studies of pyridine can confirm the Bronsted and Lewis acidity in catalysts. Fig.S4 shows the IR spectra of pyridine adsorbed on different catalysts. The peaks at 1450 and 1548 cm<sup>-1</sup> represent the Lewis acid site and Bronsted acid site, respectively. The band at 1493 cm<sup>-1</sup> was attributed to pyridine bonded to both

Lewis and Brønsted acid sites (L + B)<sup>36</sup>. The Na-MMT presents weak Brønsted acid centres and Lewis acid site. The Brønsted acidity has two sources: (1) The compensating cations, which may have a strong polarising effect on coordinated water molecules. (2) Specific sites at the layer edges: layer termination results in broken bonds which may be compensated by OH groups formation<sup>28</sup>. Coordinatively unsaturated Al and Mg are easily formed at the edges and should behave as Lewis acidic centers<sup>28</sup>. The AT-MMT presents more Brønsted acid centres and Lewis acid site. The Brønsted acid of AT-MMT was enhanced may due to two reasons. Firstly, the basal planes of MMT exposed the bridging oxides of the tetrahedral sheet which had basic properties: they also exhibited pseudo hexagonal holes within which the structural OHs of the octahedral sheet were accessible. These OH groups were very weak Brønsted acids in most clays<sup>28</sup>. However, after modified by sulfuric acid, the skeleton crystal lattice were dehisced and lamellar were delaminated, so the pseudo hexagonal holes arised and the OH groups exposed. Secondly, the interlayer cations were exchanged by H<sup>+</sup> and this protons may also enhanced the Brønsted acid. The dealumination of the framework was obvious during the acid treatment process, which we can get by the change of the compositions of different catalysts (Table S2). The increase of the unsaturated Al benefited the Lewis acid site. For PILC, one major factor may induce the increase of Lewis acid site, that is the pillars: the Al<sub>13</sub><sup>7+</sup> would lose water molecules after calcined. The Al-O-Al was created in the interlayer of MMT and the Al-O-Si was bridged with the lamellar structure. The Lewis acid site and the (L+B) were enhanced. Phosphomolybdc acid is a typical strong Brønsted acids and can offer strong option. There is no doubt that Brønsted acids strengthened for the PTMA-PILC.

### 3.7 TEM

Transmission electron microscopy was performed in order to elucidate the structure of a material. Fig. 5 shows the micrographs of the Na-MMT, AT-MMT, PILC and PTMA-PILC samples and they are greatly different. The typical TEM image of the Na-MMT represents the lamellar structure which arrange compactly and it contains a lot of metal Na<sup>+</sup> ions. After acid treatment, the impurity ions were leached out. At the same time, the layered structure disappeared and the skeleton of the MMT was disrupted, and a large number of mesoporous appeared. However, in the image of the PILC, the lamellar structure of MMT were clearly observed again. The polymerized hydroxyl ions transform aluminium oxide and dispersed adequately and uniformly in the MMT. This layer structure was able to disassembled and then assembled again in the process of acid treatment and pillaring reaction, indicating that MMT has a memory function. These changes were exactly consistent with the XRD, FT-IR and the N<sub>2</sub> adsorption-desorption isotherms. The TEM image of PTMA-PILC showed that the mesoporous layer changed little, confirming that PTMA impregnation didn't break the structure of catalyst. The PTMA particles on the surface of the catalyst were homogeneously dispersed on the catalyst surface.

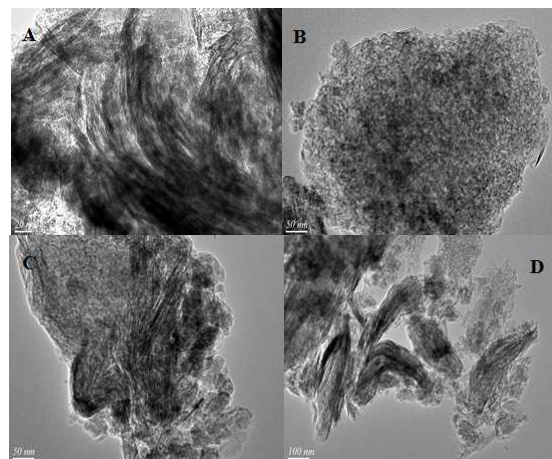
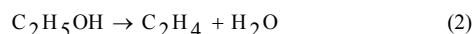


Fig. 5 TEM images of (A) Na-MMT, (B) AT-MMT, (C) PILC and (D) PTMA-PILC samples.

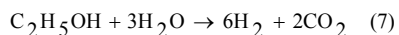
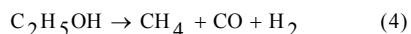
### 3.8 Catalytic Performance

The conversion of the ethanol and the selectivity to the different products over various catalysts at different temperature was shown in Fig. 6. To evaluate the reactivity of the different catalysts, the ethanol dehydration was investigated from 200 °C to 600 °C. The reactants we used simulated bioethanol which the volume fraction was just 30%. In the presence of acid catalyst, ethanol dehydrated into ethylene and water. It is known that the presence of water in the reaction could have a detrimental effect on the active sites of the solid acid catalysts. As shown in Fig. 6, at lower temperatures, the ethanol conversion was lower. With the temperature increasing, both the conversion of ethanol and selectivity towards ethylene increased for all the catalysts but reduced over different temperatures. At 500 °C, the conversion of ethanol was 16.9% for Na-MMT sample. At 400 °C, the conversion of ethanol was 74.2% for AT-MMT and 87.5% for PILC. In contrast, PTMA-PILC sample displayed the highest conversion of ethanol, up to 93.2% at lower temperature 300 °C. With four catalysts, the selectivity to ethylene showed the same change tendency. The selectivity to ethylene increased with the increasing up to a certain temperature, after which it decreased. At 200 °C, selectivity to ethylene was lower due to producing outgrowth diethyl ether. For all the catalysts, the diethyl ether formation showed a significant decline with the temperature increased, and disappeared at high temperatures. In addition, other by-products such as CH<sub>4</sub>, CO and H<sub>2</sub> appeared at this stage. As previous reports observed<sup>37</sup>, two reactions can occur in parallel during catalytic dehydration of ethanol:(Eq.(2) and Eq.(3))



The main reaction and the side reaction are endothermic and exothermic, respectively. At lower temperature, diethylether is produced in significant quantities, while at higher temperature the ethylene is the major product<sup>38</sup>. Methane may be formed during ethanol steam reforming by ethanol decomposition Eq.(4) and this

reaction is thermodynamically favored at low temperature<sup>39</sup>. For Na-MMT catalyst, the ethanol dehydrogenation (Eq.(5)) also took place during the low temperature stage of 200–400 °C, which was due to the multiple mixture of metal oxide (Table S1) of Na-MMT<sup>40-41</sup>. However, it can be seen this acetaldehyde products decreased during the process over the AT-MMT catalyst. That is because metal oxide were dissolved by the acid treating.



The ethylene formation increased distinctly as temperature go up. At higher temperature over 400 °C, the selectivity to ethylene began to decrease not only due to the formation of outgrowth produced by ethanol dehydrogenation (Eq. (5)) and acetaldehyde decomposition (Eq. (6)), but also as consequence of the steam reforming reaction of ethanol, which due to the presence of water in the feed (Eq.(7)). With Na-MMT, AT-MMT, PILC and PTMA-PILC, selectivity to ethylene was maximal (73.2%, 82.6%, 97.8%, 99.1%) at 500 °C, 400 °C, 400 °C, 300 °C, respectively. PTMA-PILC exhibited greater selectivity to ethylene than any of the catalysts at lower temperature. In summary, the conversion of ethanol and the selectivity to ethylene decreased in the order PTMA-PILC > PILC > AT-MMT > Na-MMT. In order to reveal the reason why PTMA-PILC exhibited remarkably enhanced ethylene yield in the reaction, the relations between catalytic performance of ethanol dehydration and structural properties of the catalysts were carefully considered.

Firstly, the effect of layer structure was correlated. Generally, the mesoporous/microporous structure may benefit catalysis reactions, which is mainly contributed to their enhanced diffusion features<sup>42</sup>. In our work, no direct relations between BET surface area with the ethylene yield. For example, AT-MMT possessed larger specific surface area than PTMA-PILC catalyst but showed low ethylene selectivity and ethanol conversion at low temperature

(300 °C). This was in agreement with the analysis by Hongchuan Xin<sup>43</sup>. The delamination skeleton of the MMT skeleton and recombination with the help of the  $\text{Al}_{13}^{7+}$  benefited the active centers dispersing uniformly in the MMT. PTMA were distributed homogeneously on the PILC. The PTMA-PILC and PILC possessed abundant crystal lattice defects despite that the pillaring reaction restored the lamellar structure of the MMT, which provided a large number of active centers for catalytic reaction. This may contributed to the ethanol conversion at the low temperature. What's more, the  $\text{Al}_2\text{O}_3$  phase appearing amorphous state and existing steadily in the MMT could keep high activity for the low concentration of ethanol dehydration to ethylene.

Secondly, the effect of acidity was studied. The exact chemical nature of the acid sites is still amatter of debate<sup>44-45</sup>. However, at low temperature, the relationship demonstrated that the weak acid centers most likely benefited the ethylene formation<sup>44</sup>. It is generally accepted that the primary reactions involved in the conversion of alcohol to lower hydrocarbons can occur on weak acid sites, but the subsequent reactions (e.g., oligomerization, dehydrocyclization and hydrogenation) occur on the strong acid sites with comparatively higher acid strength<sup>46-48</sup>. In addition, the Lewis and Bronsted acid sites should play an important role in the reaction. Topchieva *et al.*<sup>49</sup> suggested the dehydration of ethanol occurs essentially with the aid of Bronsted acid sites via formation of ethoxide ( $\text{C}_2\text{H}_5\text{O}^-$ ) surface species. However, according to Hussein *et al.*<sup>50</sup>, different mechanistic pathways for ethanol dehydration to diethyl ether and ethene depended largely on the surface hydroxylation. The mechanisms were listed in Supporting Information. In a number of papers, it was shown that dehydration of ethanol over solid catalysts takes place predominantly on the strength acid sites. However, the Na-MMT has a few weak Lewis acids. After modification, the most obvious change of the MMT was the change of ratio of Lewis and Bronsted acid sites. These mechanisms also admitted that the catalytic performance of catalyst in the ethanol dehydration benefited from the balance of Lewis and Bronsted acid sites.

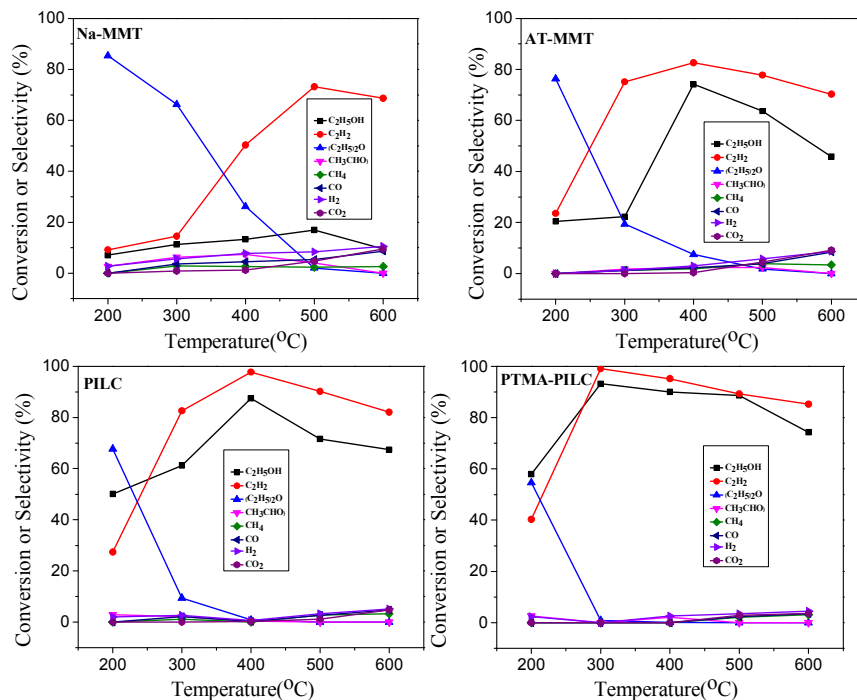
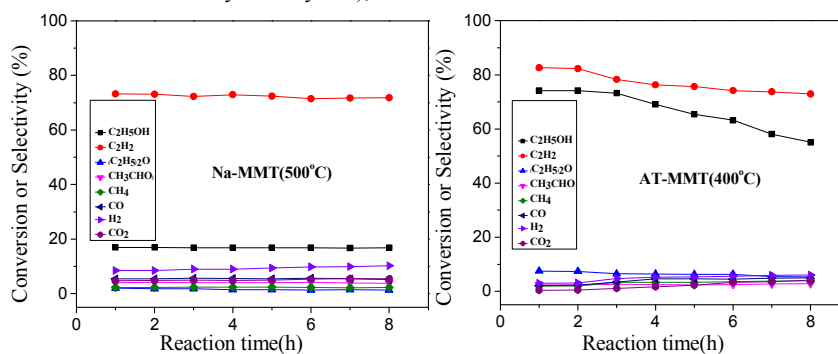


Fig. 6. The conversion of ethanol and the selectivity to the different products vs temperature over different catalysts

Due to coking and other reasons of catalyst material in catalytic reaction, catalytic activity may decrease with reaction time. In this study, the stabilities of Na-MMT, AT-MMT, PILC and PTMA-PILC catalysts were studied per hour at the optimal conditions. As can be seen in Fig.7, Na-MMT exhibited less catalytic activity but considerable stabilities, which remained unchanged for 8 h. In contrast, AT-MMT exhibited higher catalytic activity but less stability, the selectivity of ethylene reduced slowly with the extension of the time for 2 h. Compared to Na-MMT and AT-MMT catalysts, PILC and PTMA-PILC showed higher activity. The PTMA-PILC catalyst, which showed the highest initial activity (93.2% conversion of ethanol and 99.1% selectivity of ethylene),

presented slightly decrease after reaction for 6 h and remained stable. Since the reactants were simulated bioethanol, the presence of amount of water may resulted in the loss of Bronsted acids of the PTMA-PILC. In addition, the coke formation from ethylene polymerization also was considered as one reason for the catalyst deactivation. Even so, this novel catalyst exhibiting considerably high activity for the bioethanol dehydration at low temperature can build the foundation for the further catalyst research for the bioethanol dehydration.



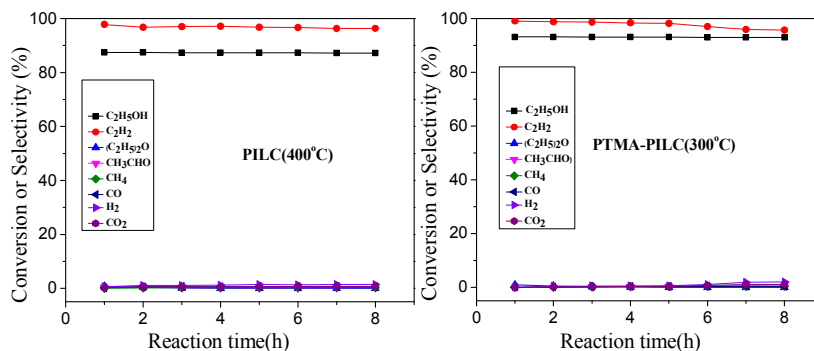


Fig. 7 The stabilities of different catalysts

## 4 Conclusions

The Na-MMT catalysts modified by acidic treatment, ion-exchanging and impregnation displayed efficient performance for the dehydration of ethanol to ethylene. The XRD patterns of the samples showed that the acid treatment would dramatically change the structure of the mineral, wherein the lamellar was delaminated in the process. The structures of surface Si\O\Si and Si\O\Al in the framework of MMT were slightly destroyed by acidic treatment. Besides, the specific surface area and pore size significantly increased. The pore size had a clear shift toward larger pore size of 9.1 nm, which was beneficial to the pillaring reaction. The structure and elementary property of MMT restored after pillared by Al<sub>13</sub><sup>7+</sup>, due to the “memory effect”. The active center dispersed uniformly and maintained stably in the MMT and the Lewis and Bronsted acid sites were further balanced by PTMA. These characteristics benefited the catalytic performance of achieving higher activity for the dehydration of ethanol to ethylene, wherein the highest catalytic activity with 93.2% conversion of ethanol and 99.1% selectivity of ethylene were obtained at the low temperature of 300 °C.

## Acknowledgments

The project was supported by the National Natural Science Foundation of China (50872086), Special/Youth Foundation of Taiyuan University of Technology (2012L022), Scientific and technological project of Shanxi Province (02010145). Scientific and technological project of Shanxi Province (2013021008-4).

## Notes and references

- 1 Y. Chen, Y. L. Wu, L. Tao, B. Dai, M. D. Yang, Z. Chen and X. Y. Zhu, *J. Ind. Eng. Chem.*, 2010, **16**, 717-722.
- 2 C. J. Pereira, *Science*, 1999, **285**, 670-671.
- 3 Y. Gucbilmez, T. Dogu and S. Balci, *Ind. Eng. Chem. Res.*, 2006, **45**, 3496-3502.
- 4 M. Zhang and Y. Yu, *Ind. Eng. Chem. Res.* 2013, **52**, 9505-9514.
- 5 V. V. Bokade, G. D. Yadav, *Appl. Clay. Sci.*, 2001, **53**, 263-271.
- 6 J. Bedia, R. Barrionuevo, J. Rodríguez-Mirasol and T. Cordero, *Appl. Catal. B-environ*, 2011, **103**, 302-310.
- 7 S. Golay, R. Doepper and A. Renken, *Appl. Catal. A*, 1998, **172**, 97-106.
- 8 J. B. Bi, X. W. Guo, M. Liu and X. S. Wang, *Catal. Today*, 2010, **149**, 143-147.
- 9 A. M. Zheng, L. Chen, J. Yang, M. J. Zhang, Y. C. Su, Y. Yue, C. H. Ye and F. Deng, *J. Phys. Chem. B*, 2005, **109**, 24273-24279.
- 10 L. D. Chen, X. S. Wang, X. W. Guo, H. C. Guo, H. O. Liu and Y. Y. Chen, *Chem. Eng. Sci.*, 2007, **62**, 4469-4478.
- 11 N. D. Feng, A. M. Zheng, S. J. Huang, H. L. Zhang, N. Y. Yu, C. Y. Yang, S. B. Liu and F. Deng, *J. Phys. Chem. C*, 2010, **114**, 15464-15472.
- 12 O. Winter and M.T. Eng, *Hydrocarb. Process.* 1976, **55**, 125-133.
- 13 X. Zhang, R.J. Wang, X.X. Yang and F.B. Zhang, *Micropor. Mesopor. Mater.* 2008, **116**, 210-215
- 14 C.B. Phillips and R. Datta, *Ind. Eng. Chem. Res.* 1997, **36**, 4466-4475.
- 15 T.M. Nguyen and R. Levanmao, *Appl. Catal.* 1990, **58**, 119-129.
- 16 Q. Sheng, K.C.Ling, Z.R. Li and L.F. Zhao, *Fuel. Process. Technol.*, 2013, **110**, 73-78.
- 17 D. Arias, A. Colmenares, M.L. Cubeiro, J. Goldwasser, C. M. Lopez, F.J. Machado and V. Sazo, *Catal. Lett.* 1997, **45**, 51-58.
- 18 A.C. Garade, V. R. Mate and C.V. Rode, *Appl. Clay. Sci.*, 2009, **43**, 113-117.
- 19 A. C. Garade, V. S. Kshirsagar, R. B. Mane, A. A. Ghalwadkar, U. D. Joshi and C. V. Rode, *Appl. Clay. Sci.*, 2010, **48**, 164-170.
- 20 M. Misono, *Catal. Rev.* 1987, **29**, 269-321.
- 21 M. Nehate and V. V. Bokade, *Appl. Clay. Sci.*, 2009, **44**, 255-258.
- 22 L. Zhang, Q. Jin, L. Shan, Y. Liu, X. Wang and J. Huang, *Appl. Clay. Sci.*, 2010, **47**, 229-234.
- 23 C. H. Zhou, *Appl. Clay. Sci.*, 2010, **48**, 1-4.
- 24 A. D. Mali, N. GShimpi and S. Mishra, *Society of Chemical Industry.* 2014, **63**, 338-346.
- 25 T. Pratyaporn and S. Punnama, *Mater Res. Bull.* 2013, **48**, 4856-4866.
- 26 J. A. Zazo, J. Bedia, C.M. Fierro, G. Pliego, J.A. Casas and J.J. Rodriguez, *Catal. Today*, 2012, **187**, 115-121.
- 27 L.A. Galeano, A. Gil and M. A. Vicente, *Appl. Catal. B*, 2010, **100**, 271-281.
- 28 J. F. Lambert and G. Poncelet, *Top. Catal.*, 1997, **4**, 43-56.
- 29 Q. Lu, X. R. Lei, Z. D. Tang and H. F. Liu, *Geological Sci. and Technology Information*, 2001, **1**, 91-98.
- 30 Y. H. Zhao, Q. Q. Hao, Y. H. Song, W. B. Fan, Z. T. Liu, and Z. W. Liu, *Energ. Fuel*, 2013, **27**, 6362-6371.
- 31 A. Paula A, B. Carolina, Q. Raúl, A. Pilar and R. H. Eduardo, *App. Catal. A*, 2013, **453**, 142-150.
- 32 K. S. W. Sing, D. H. Everett, R. A. W. Haul, L. Moscou, R. A. Pierotti, J. Rouquerol, and T. Siemieniewska, *Pure Appl. Chem.* 1985, **57**, 603-619.
- 33 M. R. Mostafa, A. M. Youssef and S. M. Hassan, *Mater Lett.*, 1991, **12**,

- 207-213.
- 34 C. B. Hedley, G. Yuan and B. K. G. Theng, *Appl. Clay Sci.*, 2007, **35**, 180-188.
- 35 F. Bergaya, A. Aouad and T. Mandalia, *Developments in Clay Sci*, 2006, **1**, 393-421.
- 36 F. Kooli, *Micropor. Mesopor. Mat.* 2014, **184**, 184-192.
- 37 G. W. Chen, S. L. Li, F. J. Jiao and Y. Quan, *Catal. Today*, 2007, **125**, 111-119.
- 38 X. Zhang, R. Wang, X. Yang and F. Zhang, *Micropor. Mesopor. Mat.*, 2008, **116**, 210-215.
- 39 M. G. Vanesa, L. Eduardo, S. Maria and L. Jordi, *J. Power. Sources*, 2009, **192**, 208-215.
- 40 V. García, E. López, M. Serra and J. Llorca, *J Power Sources*, 2009, **192**, 208-15.
- 41 V. García, E. López, M. Serra, J. Llorca and J. Riera, *Int J. Hydrogen. Energ.*, 2010, **35**, 9768-9775.
- 42 J. Perez-Ramirez, C.H. Christensen, K. Egeblad, C.H. Christensen and J.C. Groen, *Chem. Soc. Rev*, 2008, **37**, 2530-2542.
- 43 H. H. Xin, X. P. Li, Y. Fang, X. F. Yi, W. H. Hu, Y. Y. Chu, F. Zhang, A. M. Zheng, H. P. Zhang and X. B. Li, *J. Catal.*, 2014, **312**, 204-215.
- 44 W. Xia, A. Takahashi, I. Nakamura, H. Shimada and T. Fujitani, *J. Mol. Catal. A-Chem*, 2010, **328**, 114-118.
- 45 J. P. Marques, I. Gener, P. Ayrault, J. C. Bordado, J. M. Lopes, F. R. Ribeiro and M. Guisnet, *Micropor. Mesopor. Mater.*, 2003, **60**, 251-262.
- 46 K. K. Ramasamy and Y. Wang, *J. Energy Chem.* 2013, **22**, 65-71.
- 47 V. S. Nayak and V.R. Choudhary, *Appl. Catal.* 1984, **9**, 251-261.
- 48 S.N. Chaudhuri, C. Halik, J.A. Lercher, *J. Mol. Catal.* 1990, **62**, 289-295.
- 49 K.V. Topchieva, K. Yun-Pin and I.V. Smirnova, *Adv. Catal.* 1957, **9**, 799-806.
- 50 G.A.M. Hussein, N. Sheppard, M.I. Zaki and R.B. Fahim, *J. CHEM. Soc. Faraday Trans*, 1991, **87**, 2661-2668.